



ChemComm

**Multivariate Zeolitic Imidazolate Frameworks with an  
Inverting Trend in Flexibility**

Journal:	<i>ChemComm</i>
Manuscript ID	CC-COM-08-2022-004362.R1
Article Type:	Communication

SCHOLARONE™  
Manuscripts

## COMMUNICATION

## Multivariate Zeolitic Imidazolate Frameworks with an Inverting Trend in Flexibility

Arijit Halder,<sup>a</sup> Ryan A. Klein,<sup>bc</sup> Rachel Lively,<sup>a</sup> and C. Michael McGuirk<sup>\*a</sup>

Received 00th January 20xx,

Accepted 00th January 20xx

DOI: 10.1039/x0xx00000x

**Through systematic linker substitution in a flexible zeolitic imidazolate framework (ZIF) with step-shaped adsorption-desorption, structural intermediates between the known open and closed phases were isolated. Reflecting this, modulative sorption behaviour with an inverting adsorption pressure trend—in which the step pressure decreases and then increases again with increasing mixed linker concentration—is observed, highlighting how linker substitution modifies the energetic landscape of framework flexibility.**

Metal-organic frameworks (MOFs) are a large class of crystalline porous materials composed of inorganic nodes bridged by polytopic organic linkers.<sup>1</sup> Given their high achievable surface areas, modular topologies, and diverse surface chemistries, MOFs are recognized for their gas adsorption properties.<sup>2,3</sup> Most reported MOFs are structurally rigid, retaining their long-range structure upon solvent removal (*i.e.*, activation).<sup>4</sup> Depending on their pore size and shape, these frameworks typically display Type I or Type IV isothermal adsorption-desorption profiles.<sup>5</sup> In contrast, a relatively small portion of MOFs undergo a reversible phase transition upon activation to a denser crystalline phase, while retaining the underlying skeletal connectivity.<sup>6-8</sup> Importantly, these flexible (also known as soft or dynamic)<sup>9</sup> frameworks often display Type V, or “step-shaped”, isothermal adsorption-desorption profiles, characterized by minimal adsorption until some pressure threshold is reached, followed by steep uptake over a narrow pressure regime (Fig. 1b).<sup>10</sup> This behavior results from an adsorbate-induced phase transition between a low porosity

“closed” or “dense” phase to an “open” phase with greater accessible porosity (Fig. 1b). A handful of mechanisms underlying framework flexibility are known, such as gate opening and breathing, each causing an abrupt increase in accessible porosity upon the phase change. During desorption, the reverse occurs, typically with some amount of pressure hysteresis (Fig. 1b). Due to a reduced requisite pressure swing for gas uptake and release relative to rigid materials, flexible materials are attractive for a range of applications, such as H<sub>2</sub> storage, transport, and delivery.<sup>11-13</sup> Unfortunately, the discovery of flexible frameworks remains serendipitous and each framework exhibits stepped adsorption at a set point in the pressure-temperature phase space for a given adsorbate.<sup>10</sup> As such, if the adsorption-desorption profile of a new framework does not fortuitously fit the parameters of a targeted storage, transport, or separation process, then the benefits of Type V adsorption cannot be leveraged for these applications. Thus, the ability to deliberately synthetically tune the behavior of known flexible frameworks is highly desirable.

ZIF-7 (*sod*-Zn(bim)<sub>2</sub>, bim<sup>-</sup> = benzimidazolate) is a flexible framework which has been studied widely for CO<sub>2</sub> capture,<sup>14</sup> H<sub>2</sub> storage,<sup>15</sup> and olefin purification,<sup>16,17</sup> among other applications.<sup>18</sup> Yet, with this singular composition, performance has not been ideal for a given end use application. Modifying the inorganic node or organic linker while retaining the sodalite-like (*sod*-like) topology, reversible flexibility, and adsorption capacity of ZIF-7 enables realization of frameworks with synthetically tuned stepped adsorption-desorption behavior. Indeed, changing the metal ion modulates the stepped sorption of ZIF-7, with the Co(II) (ZIF-9) and Cd(II) (CdIF-13) congeners reported.<sup>19</sup> While ZIF-9 shows a mild shift to a higher step pressure for adsorption-desorption, CdIF-13 was recently reported to display an order of magnitude increase in the threshold pressure, along with much steeper sorption steps and ≈ 50 % increase in total capacity. This dramatic change has been ascribed to the longer metal-ligand bonds in the Cd(II)-based framework.<sup>19</sup>

An alternative route to tuning properties in both rigid and flexible MOF materials is a mixed-linker, or multivariate, approach.<sup>20-24</sup> In this approach a secondary linker is included in the solvothermal framework synthesis, such that it will be

<sup>a</sup> Department of Chemistry, Colorado School of Mines, Golden, Colorado, 80401 USA.

<sup>b</sup> Material, Chemical, and Computational Sciences Directorate, National Renewable Energy Laboratory, Golden, Colorado 80401, USA

<sup>c</sup> Center for Neutron Research, National Institute of Standards and Technology, Gaithersburg, Maryland 20899, USA

\*E-mail: cmmcgquirk@mines.edu

Electronic Supplementary Information (ESI) available: General and synthetic details, different isotherms, figures and tables of structural information, and details of Pawley fitting. CCDC 2194927 and 2194928. See DOI: 10.1039/x0xx00000x.

Certain commercial equipment, instruments, or materials are identified in this document. Such identification does not imply recommendation or endorsement by the National Institute of Standards and Technology, nor does it imply that the products identified are necessarily the best available for the purpose.

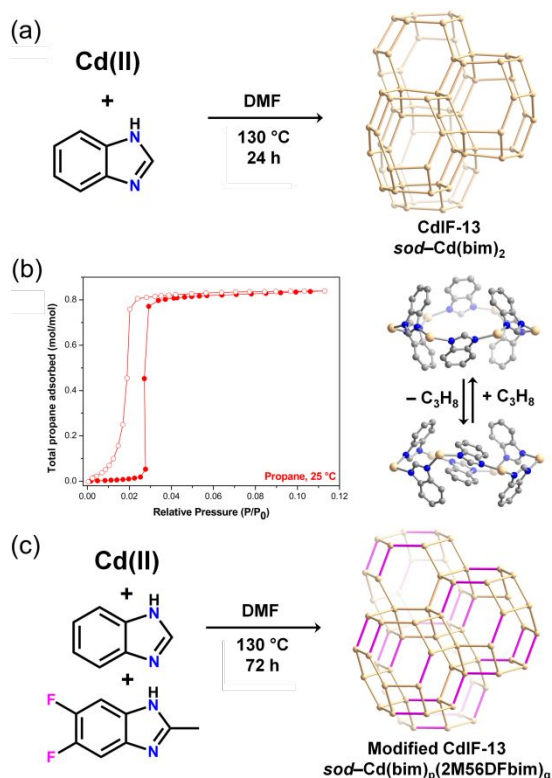


**Fig. 1.** (a) General synthetic scheme for CdIF-13 (sod-Cd(bim)<sub>2</sub>) with a topological representation of the DMF-solvated structure. Each sphere represents a tetrahedral Cd(II) node, and each line a ditopic benzimidazolate linker. (b) CdIF-13 exhibits step-shaped adsorption (closed circles) and desorption (open circles) of propane (C<sub>3</sub>H<sub>8</sub>) with minimal hysteresis. This adsorption-desorption behavior arises from a reversible phase transition between a low porosity (closed) and higher porosity (open) structure. (c) General synthetic scheme for multivariate derivatives of CdIF-13 containing varying equivalents of 2-methyl-5,6-difluorobenzimidazole. The random distribution of the secondary linker in the lattice is illustrated by the inclusion of pink lines in the topological representation. For both the synthesis, Cd(ClO<sub>4</sub>)<sub>2</sub>·xH<sub>2</sub>O is used as the Cd(II) source.

spontaneously incorporated into the framework lattice at ratios reflecting those of the synthesis conditions. This has been shown to be a powerful tool of modifying pore structure and chemistry in rigid frameworks.<sup>25</sup> In this work, we explored the ability to synthetically modify the step-shaped adsorption behavior of flexible CdIF-13 by employing this mixed-linker approach. We selected CdIF-13 for this study because: (i) its desirable capacity and step shape, (ii) both the open and closed phases are well characterized by single-crystal X-ray diffraction (SCXRD), and (iii) the adsorption process has been thoroughly studied by *in situ* powder XRD (PXRD).<sup>19</sup>

For our mixed-linker study, we targeted derivatized bim-linkers functionalized on the benzene ring and the bridging carbon of the imidazole (Figure 1c). In particular, we sought substitutions that may alter the strength of the cross-pore  $\pi$ -based interactions (benzene ring), apparent from the structure of the closed phase determined by SCXRD, and/or affect the steric accessibility of linker rotation (imidazole ring).<sup>15</sup> After screening an array of ligands, we found that introducing varying ratios of 2-methyl-5,6-difluorobenzimidazole (2M56DFbim, Fig. 1c) with the parent bim ligand during solvothermal synthesis resulted in a family of isorecticular frameworks (i.e., *sod* topology, Fig. S7). Post-digestion <sup>1</sup>H nuclear magnetic

resonance (NMR) spectroscopic measurements (Fig. S17–22) indicate a systematically varying ratio of linkers in this series of compounds (Table 1). Generally, a greater ratio of bim<sup>−</sup> is found in the framework than was used in the synthesis, which we hypothesize is due to the combined bulkiness of 2M56DFbim<sup>−</sup> and the electron withdrawing of the fluorine atoms which reduces the charge density on the imidazolate nitrogens.<sup>26</sup>

**Table 1:** Ratios of bim:2M56DFbim in the synthesis and resulting multivariate MOFs, as determined by post-digestion <sup>1</sup>H NMR spectroscopy.

Ratio in the Synthesis	1:1	1.5:1	2.3:1	3:1	4:1	9:1
Ratio in the Framework	5:4	4:1	5:1	6:1	7:1	14:1

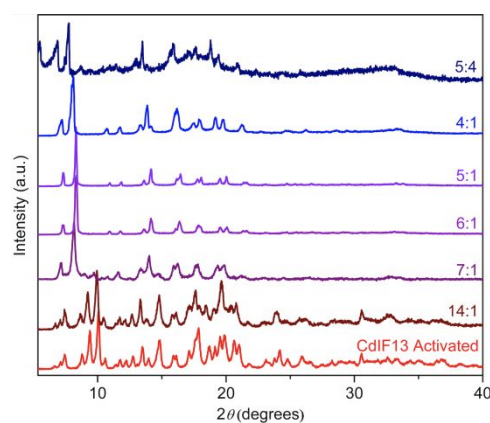


**Fig. 2.** PXRD patterns of the activated (i.e., solvent-free) multivariate derivatives of CdIF-13 with varying linker ratios. The ratios are shown as bim:2M56DFbim. For reference, the simulated pattern of activated CdIF-13, from the structure determined by SCXRD, is displayed at the bottom of the figure.  $\lambda = 1.5406 \text{ \AA}$ .

The resulting frameworks were activated under dynamic vacuum at 150 °C for 16 h. Complete solvent removal was confirmed for all frameworks using post-digestion <sup>1</sup>H NMR spectroscopy (Fig. S17–S22), except for the 5:4 (indicates ratio of bim<sup>−</sup> to 2M56DFbim<sup>−</sup> linkers) framework, which effectively traps  $\approx 0.02$  equivalents of DMF per linker in the activated structure. Thermogravimetric analysis of the activated structures shows little weight loss until  $\approx 400 \text{ } ^\circ\text{C}$  (Fig. S23).

The structures of the activated materials were then investigated using powder X-ray diffraction (PXRD) measurements (Fig. 2). Interestingly, Pawley fits of the PXRD patterns for the activated frameworks revealed that while the activated 14:1 compound is in the same  $P\bar{1}$  space group as the activated parent CdIF-13, the 7:1, 6:1, 5:1, and 4:1 materials were more structurally similar to previously characterized dichloromethane and *N,N*-dimethylformamide-solvated CdIF-13 compounds despite being fully desolvated (CH<sub>2</sub>Cl<sub>2</sub>, DMF, Fig. S42–S46, Table S2).<sup>19</sup> Further investigation via air-free PXRD measurements confirmed the activated nature of the compounds (Fig. S15).

We hypothesize that the sterically bulky methyl groups hinder complete linker rotation. This effect, combined with weakening of the cross-pore interactions by the electron-

withdrawing fluorine substituents precludes a complete phase transition to the triclinic structure seen for the closed phase of the parent CdIF-13. Instead, the 7:1, 6:1, 5:1, and 4:1 compounds are trapped in different intermediate structural

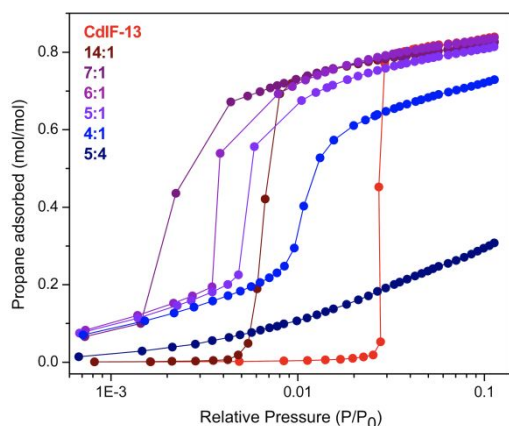


**Fig. 3** Isothermal adsorption measurements for propane ( $C_3H_8$ ) with CdIF-13 and the series of multivariate derivatives with varying linkers ratios ( $bim^-:2M56DFbim^-$ ) at 25 °C,  $P_0 = 1$  bar. The lines connecting data points are only to guide the eye and are not mathematical fits. Desorption profiles are shown in Fig. S29–31.

states between the characterized open and closed phases of CdIF-13 despite being fully activated. The progressive variation of the ligand ratio systematically alters the ground state structure of the activated frameworks, and, consequently, the framework's apparent flexibility. Importantly, the retention of flexibility upon activation for each framework was confirmed by observation of the as-synthesized phase by PXRD after re-solvating with DMF (Figs. S8–S14, S48–S52 Table S3).

Pawley fits of the PXRD pattern for the activated 5:4 framework reveal that it is also in the triclinic  $P\bar{1}$  space group, albeit with lattice parameters that are significantly modified compared to the parent CdIF-13 (Table S2, Fig S47). Moreover, the Pawley fit of the PXRD pattern for the activated 5:4 structure suggests flexibility, but to a different closed phase than activated CdIF-13 (Fig. S47). We hypothesize that the activated 5:4 structure may share some qualitative similarities with the activated parent CdIF-13, namely stabilizing  $\pi$ -based ligand–ligand interactions leading to a phase change upon activation, but further structural investigations of this material are required.

We then analyzed the relative flexibility in these materials through equilibrium isothermal adsorption–desorption measurements with propane as a probe adsorbate. CdIF-13 exhibits sharp stepped adsorption–desorption for  $CO_2$  and  $CH_4$ , but the steps occur at pressures above 1 bar, necessitating specialized instrumentation and significant sample sizes.<sup>19</sup> Therefore, propane ( $C_3H_8$ ), which is adsorbed by CdIF-13 with a pressure threshold of about 15 mbar at 25 °C (Fig. 1b, Fig. 3) was used as the probe gas for this analysis. The 14:1 framework, which by PXRD accesses a similar closed phase to CdIF-13 (Fig. 2), exhibits a significant reduction in the adsorption pressure threshold, down to  $\approx 6$  mbar, while retaining the same adsorption shape and capacity as CdIF-13 (Fig. 3). Given that there are seven linkers in the asymmetric unit cell of the

reported structure of solvent-free CdIF-13 (Fig. S41), this change is stark. We hypothesize that electrostatic repulsion between the electronegative fluorine atoms of  $2M56DFbim^-$  and the electron rich  $\pi$ -faces of the  $bim^-$  benzene rings destabilize the closed structure, causing this reduction in adsorption threshold.

In contrast to CdIF-13 and 14:1, the 7:1, 6:1, 5:1, and 4:1 activated compounds, which exist in the quasi-open monoclinic structure, display non-negligible pre-step propane adsorption (Fig. 3) which we attribute to the change in the activated structure (monoclinic vs triclinic) and the resulting relatively increased porosity of the activated structures.<sup>27</sup> At 7:1, the adsorption threshold continues to be reduced, with a minimum in the adsorption pressure threshold reached with this framework. Of interest, this step pressure of  $\approx 2$  mbar is below that reported for ZIF-7 ( $\approx 5$ –8 mbar), while displaying an  $\approx 57\%$  increase in capacity ( $\approx 0.82$  mol/mol vs.  $\approx 0.52$  mol/mol). Thus, the multivariate approach enables the tuning of adsorption step pressure for CdIF-13 below that of ZIF-7, while retaining the markedly higher capacity.

For the 6:1 and 5:1 frameworks, which have a presumed average of approximately one  $2M56DFbim^-$  ligands per asymmetric unit cell, a similar adsorption profile to 7:1 is observed, with increasing amounts of pre-step adsorption. This observation is consistent with the hypothesis that the frameworks display increasingly restrained linker rotation with increasing amounts of the  $2M56DFbim^-$  linker. Surprisingly, starting at 6:1, an inversion of the trend for adsorption threshold pressure occurs, with increasing step pressures for the increasing concentrations of  $2M56DFbim^-$ . We hypothesize that this behavior arises from decreased enthalpies of propane adsorption at the Van der Waals-based adsorption sites with increasing fluorine concentration, as well as potential attractive interactions between fluorinated linkers in the framework lattice. Additionally, these frameworks display decreasing maximum adsorption by volume, likely due to the substituent's steric repulsions.

The trend of increasing step pressure with increasing  $2M56DFbim^-$  in the framework lattice continues with the 4:1 framework. This framework shows the first evidence of lowered mol/mol adsorption capacity. We hypothesize that the methyl groups of the  $2M56DFbim^-$  linkers may fully sterically hinder one of the propane adsorption sites in the material, leading to the discontinuous decrease in overall adsorption capacity.

The effect of ligand substitution is further exemplified in the 5:4 framework. Here, no step-shaped adsorption occurs in the measured pressure window at 25 °C, and the observable capacity is dramatically reduced. The activated phase is apparently significantly stabilized by ligand–ligand interactions, or the material is effectively pore-gated to the gas at these conditions, such that the energetic barrier to pore opening is too large for propane adsorption to induce the phase change in this measured pressure window. For nitrogen adsorption, this stabilization is extended to 4:1 and 5:1 along with 5:4 framework and almost no pre-step adsorption is observed for these three frameworks (Fig. S25). To confirm that the activated 5:4 framework was still flexible, it was re-solvated with DMF,

and a return to the as-synthesized open phase was confirmed by PXRD (Fig. S13). Re-solvation with DMF and propane adsorption confirm the flexible nature of the 5:1 and 4:1 frameworks. In addition to the high phase change energy at these ratios, we hypothesize that the increased presence of the methyl groups may sterically occlude N<sub>2</sub>, blocking adsorption and causing a flat pre-step regime in the measured pressure window. While structural flexibility is apparent, the topology of the 5:4 framework is currently ambiguous given the significantly different unit cell obtained for this compound compared to the parent CdIF-13 material. Efforts are ongoing to accurately identify the structure of this derivative.

In conclusion, we demonstrate that the flexibility and adsorption properties of a porous framework can be dramatically altered using a mixed linker approach that affects the ligand interactions and behaviors thought to regulate the underlying framework phase change. For CdIF-13, we show that, at a linker ratio of 7:1 bim<sup>-</sup>:2M56DFbim<sup>-</sup>, the step pressure for propane can be lowered below that of the parent Zn congener ZIF-7 while maintaining the increased total adsorption capacity and steep step of CdIF-13. We further demonstrate that the mixed linker approach can be used to access a range of intermediate adsorption behaviors arising from a range of intermediate structures defined by modified linker rotation and inter-linker attractions.

Finally, the expansion of studied flexible frameworks through the multivariate approach augments the empirical catalogue that can be used for the development and validation of computational tools to advance the ability to predict flexibility and understand the variables that influence adsorption-desorption profiles.

A.H.: Formal analysis, investigation, writing—original draft, writing—reviewing and editing. R.A.K.: investigation, writing—review and editing. R.L.: investigation. C.M.M.: conceptualization, funding acquisition, writing—review and editing.

The views expressed in the article do not necessarily represent the views of the DOE or the U.S. Government. The U.S. Government retains and the publisher, by accepting the article for publication, acknowledges that the U.S. Government retains a nonexclusive, paid-up, irrevocable, worldwide license to publish or reproduce the published form of this work, or allow others to do so, for U.S. Government purposes. R.A.K. gratefully acknowledges the U.S. DOE Office of Energy Efficiency and Renewable Energy (EERE), Hydrogen and Fuel Cell Technologies Office (HFTO) contract no. DE-AC36-8G028308 to the National Renewable Energy Laboratory (NREL). A.H., R.L., and C.M.M. gratefully acknowledge U.S. DOE EERE HFTO award number DE-EE0008823 and Colorado School of Mines for startup funds.

There are no conflicts of interest to declare.

- 1 H.-C. Zhou, J. R. Long and O. M. Yaghi, *Chem. Rev.*, 2012, **112**, 563–564.
- 2 J. Y. Lee, D. H. Olson, L. Pan, T. J. Emge and J. Li, *Adv. Funct.*

- Mater.*, 2007, **17**, 1255–1262.
- 3 J.-R. Li, R. J. Kuppler and H.-C. Zhou, *Chem. Soc. Rev.*, 2009, **38**, 1477–1504
- 4 J. R. Long and O. M. Yaghi, *Chem. Soc. Rev.*, 2009, **38**, 1213–1214.
- 5 J. Rouquerol, F. Rouquerol, P. Llewellyn, G. Maurin and K. S. Sing, *Adsorption by powders and porous solids: principles, methodology and applications*, Academic press, 2nd edn, 2013.
- 6 H. J. Choi, M. Dinca and J. R. Long, *J. Am. Chem. Soc.*, 2008, **130**, 7848–7850.
- 7 T. K. Trung, P. Trens, N. Tanchoux, S. Bourrelly, P. L. Llewellyn, S. Loera-Serna, C. Serre, T. Loiseau, F. Fajula and G. Férey, *J. Am. Chem. Soc.*, 2008, **130**, 16926–16932.
- 8 Y. Liu, J.-H. Her, A. Dailly, A. J. Ramirez-Cuesta, D. A. Neumann and C. M. Brown, *J. Am. Chem. Soc.*, 2008, **130**, 11813–11818.
- 9 S. Krause, N. Hosono and S. Kitagawa, *Angew. Chem., Int. Ed.*, 2020, **59**, 15325–15341.
- 10 A. Schneemann, V. Bon, I. Schwedler, I. Senkovska, S. Kaskel and R. A. Fischer, *Chem. Soc. Rev.*, 2014, **43**, 6062–6096.
- 11 M. P. Suh, H. J. Park, T. K. Prasad and D.-W. Lim, *Chem. Rev.*, 2012, **112**, 782–835.
- 12 R. A. Klein, H. A. Evans, B. A. Trump, T. J. Udovic and C. M. Brown, Neutron scattering studies of materials for hydrogen storage, in Reference Module in Chemistry, Molecular Sciences and Chemical Engineering, Elsevier, 2021, ISBN 9780124095472, DOI: 10.1016/B978-0-12-823144-9.00028-5
- 13 L. J. Murray, M. Dincă and J. R. Long, *Chem. Soc. Rev.*, 2009, **38**, 1294–1314.
- 14 X. Wu, M. N. Shahrak, B. Yuan and S. Deng, *Microporous Mesoporous Mater.*, 2014, **190**, 189–196.
- 15 R. A. Klein, S. Shulda, P. A. Parilla, P. Le Magueres, R. K. Richardson, W. Morris, C. M. Brown and C. M. McGuirk, *Chem. Sci.*, 2021, **12**, 15620–15631.
- 16 C. Gucuyener, J. van den Bergh, J. Gascon and F. Kapteijn, *J. Am. Chem. Soc.*, 2010, **132**, 17704–17706.
- 17 J. M. Falkowski, P. I. Ravikovitch, M. S. Abdulkarim, G. M. Muraro, S. F. Liu, C. Paur, E. A. Strohmaier and S. C. Weston, *J. Mater. Chem. A*, 2022, **10**, 1425–1432
- 18 A. Arami-Niya, G. Birkett, Z. Zhu and T. E. Rufford, *J. Mater. Chem. A*, 2017, **5**, 21389–21399.
- 19 C. M. McGuirk, T. Runčevski, J. Oktawiec, A. Turkiewicz, M. K. Taylor and J. R. Long, *J. Am. Chem. Soc.*, 2018, **140**, 15924–15933.
- 20 R. Banerjee, H. Furukawa, D. Britt, C. Knobler, M. O’Keeffe and O. M. Yaghi, *J. Am. Chem. Soc.*, 2009, **131**, 3875–3877.
- 21 T. Lescouet, E. Kockrick, G. Bergeret, M. Pera-Titus, S. Aguado and D. Farrusseng, *J. Mater. Chem.*, 2012, **22**, 10287–10293.
- 22 J.-S. Qin, S. Yuan, Q. Wang, A. Alsalme and H.-C. Zhou, *J. Mater. Chem. A*, 2017, **5**, 4280–4291.
- 23 J.-P. Zhang, A.-X. Zhu, R.-B. Lin, X.-L. Qi and X.-M. Chen, *Adv. Mater.*, 2011, **23**, 1268–1271.
- 24 S. Yuan, W. Lu, Y.-P. Chen, Q. Zhang, T.-F. Liu, D. Feng, X. Wang, J. Qin and H.-C. Zhou, *J. Am. Chem. Soc.*, 2015, **137**, 3177–3180.
- 25 S. Nandi, S. Wang, M. Wahiduzzaman, V. Yadav, K. Taksande, G. Maurin, C. Serre and S. Devautour-Vinot, *ACS Appl. Mater. Interfaces*, 2021, **13**, 20194–20200.
- 26 J. López-Cabrelles, E. Miguel-Casañ, M. Esteve-Rochina, E. Andres-Garcia, I. J. Vitorica-Yrezabal, J. Calbo and G. M. Espallargas, *Chem. Sci.*, 2022, **13**, 842–847.
- 27 M. Åhlen, A. Jaworski, M. Strømme and O. Cheung, *Chem. Eng. J.*, 2021, **422**, 130117.

Journal Name

COMMUNICATION